Scaling behavior of three-dimensional dendrites

Q. Li and C. Beckermann*
Department of Mechanical Engineering, The University of Iowa, Iowa City, Iowa 52242
(Received 8 September 1997)

The scaling behavior of geometry parameters in three-dimensional dendritic growth is investigated through a detailed measurement of the morphology of pure succinonitrile dendrites grown on the first microgravity flight of the isothermal dendritic growth experiment [M. E. Glicksman, M. B. Koss, and E. A. Winsa, Phys. Rev. Lett. **73**, 573 (1993)]. Measurements are performed of the integral parameters of a sidebranching dendrite, such as the envelope shape, projection area, contour length, volume, surface area, and solid volume fraction. The evidence presented here reveals that unique scaling relations exist between these geometry parameters and the primary tip radius or speed in steady growth. These relations are valid far away from the tip, up to a normalized distance equal to about the inverse of the tip Péclet number. For the secondary arm envelope on the sidebranch plane, a self-similar scaling behavior given by $X_{\mathrm{tip}}/R=0.668(Z/R)^{0.859}$ is found, where X_{tip} is the envelope width (or the secondary dendrite tip position), Z is the distance away from the primary tip, and R is the primary tip radius. The normalized projection area F/R^2 and the normalized contour length U/R demonstrate an identical time dependence after some initial transient, which indicates that the interfacial length concentration U/F is time independent and inversely proportional to the tip radius R. The volume V and the surface area A of a dendrite can also be scaled to the primary tip radius R. It is noted that the interfacial area concentration A/V has a similar behavior and the same order value as U/F. The experimental results are compared to analytical predictions [E. Brener and D. Temkin, Phys. Rev. E **51**, 351 (1995)] and generally found to be in good agreement. Finally, the internal solid volume fractions for various envelopes are deduced from the volume measurements and found to be in good agreement with a simple heat transfer model. [S1063-651X(98)03403-5]

PACS number(s): 81.10.Aj, 81.10.Mx, 81.30.Fb

I. INTRODUCTION

Dendrites are the most frequently observed growth mode when an alloy is solidified in a supercooled melt and are encountered in most casting and welding processes. The nonlinear growth processes leading to the spontaneous formation of such a complicated pattern have been the subject of many theoretical, numerical, and experimental investigations [1–6].

The analysis of dendritic solidification is complex because of the multitude of mechanisms that are responsible for the development of the microstructure. Two stages can be distinguished in dendritic solidification: (i) the steady-state propagation of the tip region, accounting for the formation of the main or primary stem, and (ii) the time-dependent evolution of the secondary and tertiary sidebranches, a process that leads to the formation of a dendrite envelope and establishes the more obvious length scales of a dendrite. The tip is the best-studied region of the dendrite. A number of theories have been developed for describing the steady-state growth of a single, branchless dendrite tip into an infinite, motionless, supercooled liquid [7–9]. Experimentally, the use of transparent model substances such as succinonitrile (SCN) has facilitated dendritic growth studies where tip velocities and shapes could be accurately measured and then used as a test of theory. In particular, the isothermal dendritic growth experiment (IDGE) of Glicksman, Koss, and Winsa [10], conducted under microgravity conditions, has generated benchmark data for the validation of theories that consider diffusional transport of heat only.

While the steady growth of a single dendrite tip in a uniformly supercooled melt is reasonably well understood, much remains to be learned about the evolution of dendrite sidebranches away from the tip. In fact, a good understanding of the sidebranch features and development is important for improving the engineering properties of materials that solidify dendritically because it is these sidebranches that establish the length scales and pattern of microsegregation. Curiously, until recently, the time-dependent behavior of sidebranches was ignored in most theories and there are many questions that are not fully answered at the moment. What is the branching mechanism? Do scaling parameters exist that can characterize the sidebranches (or the whole dendrite) other than the sidebranch spacing, which is generally very difficult to measure in experiments? Is there a relationship between the steady-state growth of the dendrite tip and the time-dependent growth of the sidebranches? In other words, can the lengths further back from the tip also be scaled with the tip radius R?

In this paper we shall restrict our attention to the study of the sidebranch evolution of single SCN dendrites that grow freely into a three-dimensional volume of supercooled melt. Using images from the microgravity experiments of Glicksman *et al.*, we have measured not only the tip velocity v_t and the tip radius R, but also the secondary dendrite tip position X_{tip}, the projection contour length U, and the projection area F as a function of the distance from the primary tip Z in the supercooling range $0.2<\Delta T<0.7$ K. From these measure-

*Author to whom correspondence should be addressed. FAX: 319-335-5669. Electronic address: becker@icaen.uiowa.edu

ments, a simple model, based on some physical assumptions and geometry approximations, has been developed for estimating the volume V and the surface area A of dendrites. Finally, the behavior of two important integral parameters, the interfacial area concentration S and the volume fraction f_v, are derived from the measurements. Because the experiments were performed in a microgravity environment where gravity-driven convection was absent, our results can help in the verification of existing theories and guide in the development of theories that consider diffusional transport of heat only.

II. PREVIOUS WORK

Tiller and co-workers [11] performed one of the first quantitative investigations of dendrite sidebranch evolution. An early successful model of the sidebranch evolution appears to be Langer and Müller-Krumbhaar's marginal stability theory [12–14], which ascribes the evolution of sidebranches to an intrinsic morphological instability of the needle dendrite, with the possible exception of the tip itself, where the system could persist in a marginal state of interfacial stability. Later, Huang and Glicksman [4] carried out a systematic experimental investigation of the sidebranch evolution of SCN dendrites. Their results provided insight into such fundamental problems as the origin of sidebranch perturbations, the mechanism of sidebranch evolution, and the dynamics of sidebranch coarsening. The measurements were limited to the spacing of sidebranches only and cannot give any information about other important parameters such as the dendrite envelope geometry, the solidified volume, and the surface area.

After these notable pioneering studies, more detailed experiments investigating the typical sizes of sidebranches have been performed in thin growth vessels with a thickness comparable to the tip radius. Two types of experiments can be distinguished among these two-dimensional growth studies: (i) dendrites growing without disturbance from the outside of the growth vessel [15] and (ii) dendrites where the growth of the sidebranches was forced by external mechanisms such as heat pulses [6] or the oscillating flow of a solution [16]. An important finding from these experiments is that in the absence of an external disturbance, irregular sidebranches are observed, the wavelength is not well defined, and the correlation between opposite sides of the dendrite is weak; oppositely, in the presence of external perturbations, a region of regular sidebranches with a correlation between sidebranches on opposite sides is observed. The two-dimensional experimental results suggest that in three-dimensional dendritic growth the sidebranches of dendrites grown on ground would be more regular, because the natural convective flow acts as an external disturbance, than those grown in a microgravity environment.

Theoretically, Langer and co-workers extended the analytical techniques of Barbieri, Hong, and Langer [17] for the steady-state selection problem to the dynamic problem of dendritic sidebranching in both a two-dimensional [18] and three-dimensional symmetric model [19]. The basic assumption is that sidebranching is driven by selective amplification of noise near the tip. The results of the three-dimensional analysis show that (i) the root-mean-square amplitude of sidebranches generated by thermal fluctuations grows exponentially as a function of $[(r/R)(1/\sigma)]^{1/2}$, where R is the tip radius, r is the radial distance between a symmetric steady-state paraboloidal needle crystal $Z/R=\frac{1}{2}(r/R)^2$ and the interface in cylindrical coordinates $r\equiv(r,\phi)$ and Z, and σ is a stability constant; (ii) the characteristic wavelength (the sidebranch spacing), in units of the tip radius, is

$$\frac{\lambda}{R}=\pi\left(6\sigma\,\frac{r}{R}\right)^{1/2}; \tag{2.1}$$

and (iii) the relative width of the frequency distribution is $\Delta\omega/\omega_0=(3\sigma/8r/R)^{1/4}$, i.e., the frequency distribution becomes sharper with increasing radial distance from the tip r.

By comparing the above theoretical predictions with the experimental results of Huang and Glicksman [4], Langer found that purely thermal noise seems to be too small by one to two orders of magnitude. However, the two-dimensional model, which uses the same analytical technique and is based on the same physical assumptions as the three-dimensional theory, is in good agreement with two-dimensional experiments [6,15,16]. This inconsistency shows that three-dimensional dendrites are by far not as well understood as two-dimensional dendrites.

Recently, an approach has been developed by Hurlimann *et al.* [20] to experimentally investigate dendritic growth with special emphasis on the development of sidebranches and the coarsening process in regions far away from the dendrite tip. They found that those parameters that characterize the sidebranches as independent parts of the dendrite, e.g., the length, the amplitude, and the spacing of the sidebranches, are not adequate parameters to describe the complex shape of a dendrite. Therefore, an alternative set of parameters was proposed: the contour length U, the projection area F, and the volume V of a dendrite, in order to characterize the integral behavior of the dendrite. Their experimental results for xenon dendrites show that these parameters are well reproducible and give two interesting relationships: (i) F increases linearly with U, while the slope m is proportional to R and (ii) the volume V of dendrites increases with L^3 (i.e., the length of a dendrite) and R, i.e., $V\propto RL^3$. These scaling relations are supercooling independent, implying that the dendrites are self-similar in the sidebranching region. Although the above-mentioned experiments were carried out in gravity and in a very low supercooling regime ($0.025\ \mathrm{K}<\Delta T<0.170\ \mathrm{K}$) and the conclusions have not yet been confirmed by other independent experiments, the idea of using such integral parameters as a set of indicators of overall dendritic growth behavior does represent a promising starting point for further studies of dendritic solidification.

Another important result in dendritic growth theory is the whole needle-crystal solution for three-dimensional (3D) dendritic growth, recently obtained by Brener [21]. For the tip region, the existing 3D nonaxisymmetric model developed by Ben Amar and Brener [22] was used. The selected tip shape can be written, in cylindrical coordinates, as

$$\frac{Z}{R}\left(\frac{r}{R},\phi\right)=-\frac{(r/R)^2}{2}+\sum A_m(r/R)^m\cos(m\phi). \tag{2.2}$$

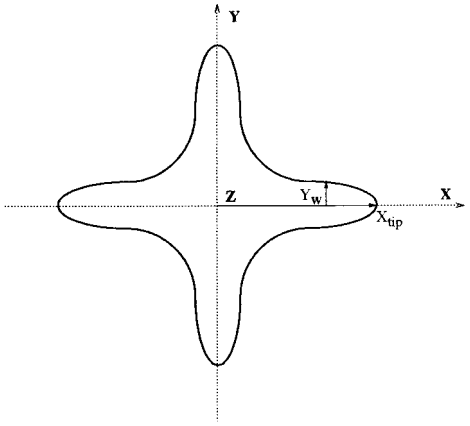

FIG. 1. Schematic representation of a cross section of a 3D needle crystal at a given distance from the primary tip Z.

For a crystal with fourfold cubic symmetry, the first nonnegligible correction term to the parabola (Ivantsov solution [23]) is the fourth-order harmonic ($m=4$, $A_4=\frac{1}{88}$). Brener described the tail region behind the tip as a time-dependent two-dimensional problem of the motion of the cross section of the 3D tail. He found that if the size of the 2D pattern (the cross section of the tail) is much smaller than a diffusion length $(\alpha t)^{1/2}$, the diffusion field of the cross section satisfies the Laplace equation. This 2D Laplacian problem was solved recently, both numerically and analytically, by Almgren, Dai, and Hakim [24], who were interested in anisotropic Hele-Shaw flow. Introducing their results to the 3D dendrite problem, the intermediate asymptotic tail shape is given in the form of the arm width Y_w in Cartesian coordinates (X,Y,Z) (as shown schematically in Fig. 1):

$$\frac{Y_w}{R}\left(\frac{X}{R},\frac{Z}{R}\right)=\left(\frac{5}{3}\frac{Z}{R}\right)^{2/5}\left(\frac{\sigma}{\sigma_2}\right)^{1/5}\left(\frac{X}{X_{\rm tip}}\right)^{2/3}\int_{x/x_{\rm tip}}^{1}\frac{ds}{s^{2/3}\sqrt{1-s^4}} \tag{2.3}$$

so that the tip position of the arms $X_{\rm tip}$ is given by

$$\frac{X_{\rm tip}}{R}=\left(\frac{5}{3}\frac{Z}{R}\right)^{3/5}\left(\frac{\sigma}{\sigma_2}\right)^{1/5}, \tag{2.4}$$

where $\sigma_2\approx\sigma$.

The above needle-crystal solution does not account for noise-induced sidebranching behavior. The description of this behavior needs the solution of a time-dependent problem for the noise-induced perturbation around the needle-crystal shape [19]. Taking into account the nonaxisymmetric shape of a three-dimensional needle crystal and using an analytical approach similar to Langer [19], Brener and Temkin [25] then studied the time-dependent behavior of sidebranch formation. According to Brener and Temkin, the root-mean-square amplitude of sidebranches generated by thermal fluctuations grows exponentially as a function of $Z^{2/5}/\sigma^{1/2}$, which is faster than in the axisymmetric case where the amplitude grows exponentially as a function of $Z^{1/4}/\sigma^{1/2}$. This important result is able to resolve the puzzle that experimentally observed sidebranches have much larger amplitudes than can be explained by thermal noise in the framework of the axisymmetric approach.

Brener and Temkin [25] also discussed the strongly nonlinear growth behavior of sidebranches far away from the tip, but where the sidebranches do not yet behave as free dendrites. This self-similar regime has a large range for small Pe, given by $1\ll Z/R\ll 1/\mathrm{Pe}$, where $\mathrm{Pe}=v_tR/2\alpha$ is the tip Péclet number, v_t is the tip speed, and α is the thermal diffusivity. The competition between the sidebranches leads to a spacing $\lambda_s(Z/R)$ between the surviving or ''active'' sidebranches that is of the same order of magnitude as the length of the sidebranches $l_s(Z/R)$. By estimating the temperature field far away from the dendrite, using energy conservation arguments, and assuming the selection criterion for the sidebranch tips to be the same as for a free dendrite, Brener and Temkin arrived at the scaling relations

$$\lambda_s(Z/R)\sim l_s(Z/R)\sim s(Z/R)\sim Z/R, \tag{2.5}$$

where s is the cross sectional area of a branch. These relations imply that dendritic structures far from the primary tip can be described by supercooling independent geometric parameters that are scaled with the primary tip radius, as already suggested by the experimental work of Hurlimann *et al.* [20].

The fact that dendrites, even far from the tip, are self-similar and can be scaled with R was further confirmed by the experimental work of Bisang and Bilgram [26,27] on xenon dendrites. They showed that the fractal dimension of the contour of a sidebranching dendrite is the same (equal to 1.42) for all supercoolings over a range of more than two orders of magnitude in length scale. Obviously, the fractal dimension is of the same nature as the integral parameters used by Hurlimann *et al.* [20]. Bisang and Bilgram [26,27] were also able to experimentally verify the tip shape relation (2.4) derived by Brener [21] as well as the position of the first sidebranch theoretically predicted by Brener and Temkin [26]. The key conclusion from the latter finding is that sidebranches are indeed initiated by thermal fluctuations.

Since the experimental work of Hurlimann *et al.* [20] and Bisang and Bilgram [26,27] was limited to xenon dendrites, it is important to verify the scaling relations reviewed above for another substance under different conditions and for other parameter ranges. The microgravity data for SCN of Glicksman, Koss, and Winsa [10] provide this opportunity. In this paper we focus on the sidebranch behavior far from the tip, as this is the least studied region of a dendrite.

III. IMAGE ANALYSIS TECHNIQUE

The images used in this investigation come from the IDGE launched by NASA in 1994 as part of the United States Microgravity Payload (USMP-2). The IDGE experiments were performed using ultrapure SCN. The process of growing a dendrite starts by melting the SCN and lowering the bath temperature to the desired supercooling. Once the system thermally stabilizes at a predetermined supercooling level, a thermoelectric cooler is activated to initiate dendritic growth. At this point, 35-mm photographs are taken at regular time intervals along two perpendicular optical paths. For

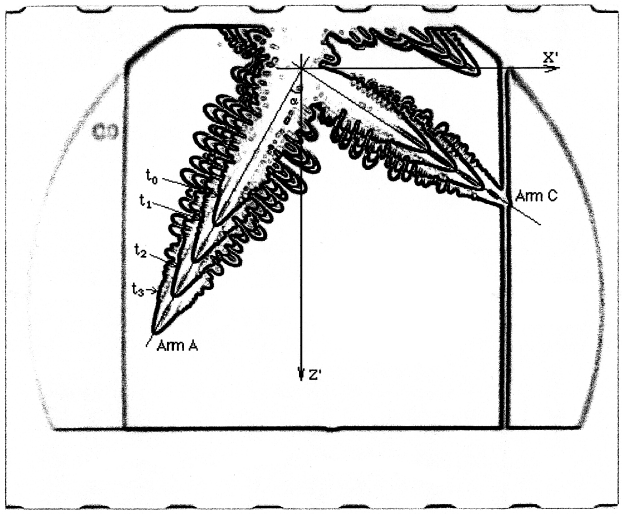

FIG. 2. Superimposed dendrite images taken at different times (IDGE USMP-2 flight, $\Delta T = 0.370$ K, view 2). The time interval between the images is 83.25 sec.

more detail about the IDGE experiment, please refer to Refs. [10,28–31].

The photographs in the form of pairs of digitized binary images serve as the primary source of 3D dendrite information used in this investigation. They are processed and analyzed in the following manner.

As a first step, the images taken at the same supercooling and from the same view but at different times are superimposed into one image (Fig. 2). Once the tip positions of different primary arms at different times are located in the superimposed dendrite image, it is easy to measure the projected angle α between the primary arm and the stinger axis direction (indicated by Z' in Fig. 2) as seen in each of the two orthogonal images. Knowing a pair of such projected angles measured in the two perpendicular views for the same arm, we can determine the orientation of this arm, i.e., the Eulerian angle of the growth velocity vector with respect to a coordinate system aligned with the stinger tube axis, as well as the orientation of one sidebranch plane. Due to the fourfold rotational symmetry, it does not matter which of the four sidebranch planes is used.

After the orientation of the dendrite is determined, the solid-liquid interface is tracked by marking it with a sufficient number of points such that the root region of the sidebranches can be identified. Then the coordinates of the points on the interface are transformed by rotation and translation in such a way that the tip of the stinger is located at the origin, the studied sidebranch plane is placed in the XZ plane of the frame of reference, and the symmetry axis of one primary arm is oriented along the Z axis (see Fig. 3). From this two-dimensional reconstruction, we make a preliminary fit of the tip region with a second-order polynomial equation and determine more accurately the tip locations at different times. The tip speed can then be deduced from this procedure by plotting the tip displacement versus times. The values listed in Table I are the same as those obtained by Glicksman *et al.* [29].

Using the more accurate tip coordinates obtained from the above method, we further translate the coordinate system so that all tips are located at the origin (see Fig. 4). After this

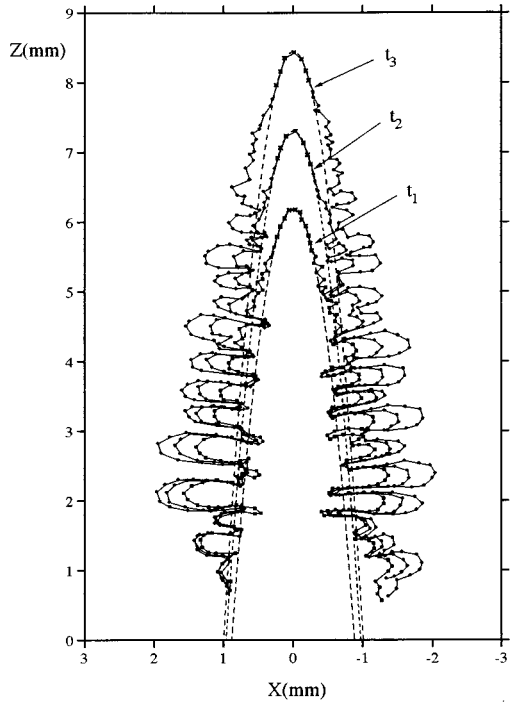

FIG. 3. Dendrite arm A reconstructed from the images in Fig. 2 and rotated to lie in a sidebranch plane. The interrupted lines are the parabolas fitted to the tip.

transformation, the positions of the secondary dendrite tips can be easily identified (Fig. 4). Also, a more accurate parabola is fitted to the tip to determine the tip radius R. Since the tip shape is not exactly paraboloidal, the values of the tip radius R, deduced from the parabola fit, depend on the distance away from the tip Z, where the parabola is fit. Using a regression technique as in Ref. [31], we then determined the tip radius R by extrapolating the values of R to $Z = 0$. In spite of basing the present measurements on relatively low-resolution digital images, the present tip radii are in reasonable agreement with the results of Glicksman *et al.* [29] who used much-higher-resolution images (see Table I). Because the tip radius measurements of Glicksman *et al.* are more accurate, they are used in the following sections. The lower resolution of the present images is not expected to influence the measurement of the other quantities, as described next.

The measurements of the contour length U and the projection area F are performed using appropriate image analysis software with area and length measurement functions. U is the length of the contour of the dendrite measured from the tip to a distance Z further back. F is one-half of the area of the projection of the dendrite as shown in Fig. 5. The quantities F and U are measured for both sides of the dendrite. Since the sidebranches do not always grow normal to the Z axis and their shapes are very complicated, U and F cannot be defined in a unique way everywhere as a function of Z. Thus we only measure the values of F and U between the tip and the points designated by dots in Fig. 5, which correspond to valleys between two neighboring sidebranches. This way, the functions $F(Z)$ and $U(Z)$ are well defined.

An attempt is made to estimate the volume and surface area of a 3D dendrite, based on a combination of actual measurements and some approximations. First, a 3D dendrite

TABLE I. Tip radius R and speed v_t for the four experiments analyzed in the present study: comparison between the results of Glicksman *et al.* [30] and our measurements.

Results	$\Delta T = 0.287$ K	$\Delta T = 0.370$ K	$\Delta T = 0.470$ K	$\Delta T = 0.609$ K
R (μm), Glicksman *et al.*	59	44	34	25
R (μm), our results from low-resolution images (not used)	61	47	38	30
v_t (μm/sec), our results and those of Glicksman *et al.* are identical	8.4	13.6	22.7	44.1

can be considered as a combination of a primary stem and secondary sidebranches. The total volume V_{total} (or total surface area A_{total}) consists, therefore, of the volume V_{stem} (or surface area A_{stem}) of the primary stem and the volume V_{bran} (or surface area A_{bran}) of the sidebranches:

$$V_{\text{total}} = V_{\text{stem}} + V_{\text{bran}}, \tag{3.1a}$$

$$A_{\text{total}} = A_{\text{stem}} + A_{\text{bran}}. \tag{3.1b}$$

The primary stem can be approximated by a paraboloid of revolution ($r^2 = 2RZ$). Its volume and surface area are then given by

$$V_{\text{stem}} = \int_0^Z \pi r^2 dZ = \pi R Z^2, \tag{3.2a}$$

$$A_{\text{stem}} = \tfrac{2}{3}\pi R^2[(1+2Z/R)^{3/2} - 1]. \tag{3.2b}$$

Now the problem is how to estimate the secondary sidebranch volume and surface area. The following approximations are made in this calculation. (i) Any secondary sidebranch i around the primary stem is also approximated by a paraboloid of revolution with a tip radius R_i and a length L_i. (ii) The sidebranches are assumed to be periodic with a wavelength (spacing) λ that varies as a function of Z. (iii) The sidebranches grow normal to the symmetry axis (Z axis). Now the key issue is the determination of the secondary arm spacing λ.

As mentioned in Sec. II, Langer [19] has predicted, through Eq. (2.1), the behavior of the branch spacing in his three-dimensional symmetric model. Transforming r (the radial distance from the tip for the Ivantsov parabola) into Z (the axial distance away from the tip) and using the stability constant $\sigma \approx 0.02$ [4], we have

$$\lambda/R = \pi(6\sigma)^{1/2}(2Z/R)^{1/4} \approx 1.29(Z/R)^{0.25}. \tag{3.3}$$

This equation indicates that the secondary sidebranch spacing can be correlated to the distance away from the tip by a power law $\lambda/R = a(Z/R)^b$, with an exponent of 0.25. By

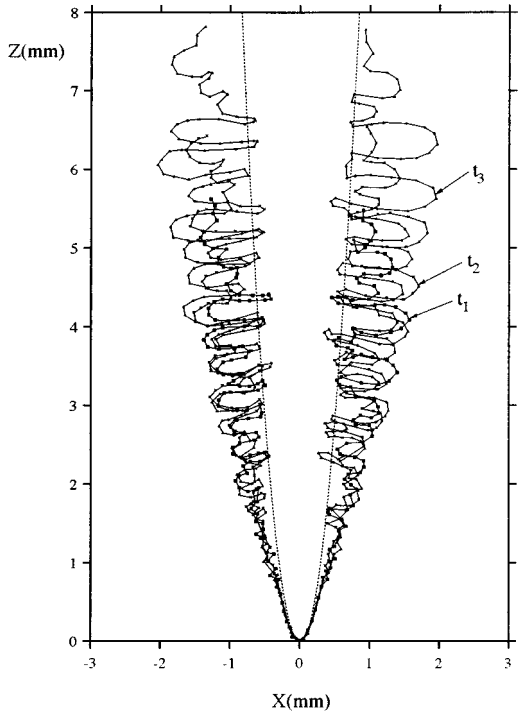

FIG. 4. Transformation of Fig. 3 realized by locating all primary tips at the origin of the coordinate system. The interrupted line is the tip parabola with $R = 44$ μm.

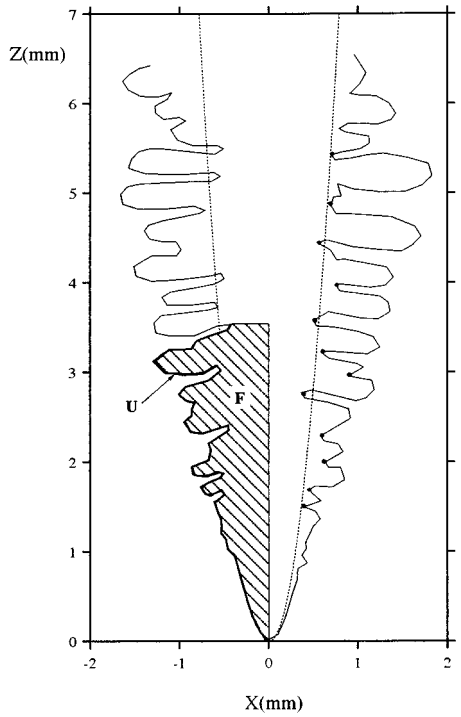

FIG. 5. Definitions of the projection area F and the contour length U. The hatched area marks the area of projection F. The arc length of the contour measured from the tip to the end of the hatching represents the corresponding contour length U.

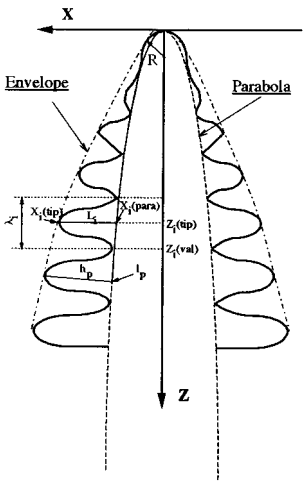

FIG. 6. Schematic representation of some symbols involved in the calculation of dendrite volume and surface area.

comparing the initial sidebranch spacing predicted by Eq. (3.3) with the experimental results of Huang and Glicksman [4], we found that the predicted value $\lambda/R \approx 2.1$ is slightly lower than the measured $\lambda/R \approx 3$. Adjusting the constant a in Eq. (3.3) and making it consistent with the experimental data of Huang and Glicksman, we obtain

$$\lambda/R \approx 1.69(Z/R)^{0.25}. \tag{3.4}$$

In our investigation, we have tried to measure the secondary sidebranch spacing λ as a function of Z, including all sidebranches. Although these measurements are very difficult due to the irregularity of the sidebranches of the dendrites grown in microgravity, our preliminary results seem to be consistent with the prediction of Eq. (3.4). A more detailed discussion of this issue will be provided in another paper [32]. The above adjusted equation is used in the following to estimate the λ values in the calculation of the volume and surface area of the dendrite sidebranches.

Assuming that the first sidebranch occurs at $Z_1(\text{tip})/R = 10$, the z-axis value of every sidebranch tip $Z_i(\text{tip})$ and valley $Z_i(\text{val})$ can be determined from Eq. (3.4). The length L_i of a sidebranch can be obtained from the shape of the sidebranch envelope by taking the difference between the envelope width $X_i(\text{tip})$ and the corresponding width $X_i(\text{para})$ of the parabola fitted to the primary arm tip, i.e., $L_i = X_i(\text{tip}) - X_i(\text{para})$. Figure 6 gives schematically the definition of all symbols involved here. Knowing the sidebranch length L_i and spacing λ_i, the volume and surface area can be determined according to the paraboloid description. The total volume V_{bran} and surface area A_{bran} are obtained by summing all sidebranches placed on the four sidebranch planes as

$$V_{\text{bran}} = 4\sum_1^n \pi R_i L_i^2 = 4\sum_1^n \frac{\pi}{8}\lambda_i^2 L_i, \tag{3.5a}$$

$$A_{\text{bran}} = 4\sum_1^n \frac{2}{3}\pi\left(\frac{\lambda_i^2}{8L_i}\right)^2\left[\left(1+16\frac{L_i^2}{\lambda_i^2}\right)^{3/2}-1\right]. \tag{3.5b}$$

Therefore, the total volume of the dendrite at the valley $Z_n(\text{val})$ is given by

$$V_{\text{total}} = \pi R Z_n^2(\text{val}) + 4\sum_1^n \frac{\pi}{8}\lambda_i^2 L_i \tag{3.6a}$$

and the total surface area A_{total} is

$$A_{\text{total}} = \frac{2}{3}\pi R^2\left[\left(1+2\frac{Z_n(\text{val})}{R}\right)^{3/2}-1\right] + 4\sum_1^n \frac{2}{3}\pi\left(\frac{\lambda_i^2}{8L_i}\right)^2\left[\left(1+16\frac{L_i^2}{\lambda_i^2}\right)^{3/2}-1\right] - 4\sum_1^n \pi(\lambda_i/2)^2, \tag{3.6b}$$

where the quantity $4\Sigma_1^n \pi(\lambda_i/2)^2$ is the area occupied by the sidebranches on the primary stem and is subtracted in the total surface area calculation.

IV. RESULTS AND DISCUSSIONS

A. Shape of the sidebranch envelope

An important parameter for characterizing the complex morphology of a dendrite far from the tip is the envelope of the growing sidebranches. This envelope represents a smooth connection of all the ''active'' or surviving sidebranch tips, where a branch is judged as active when it is longer than the next active branch closer to the tip. Its shape can be described by the secondary tip positions X_{tip} (the distance away from the primary axis) as a function of the distance from the primary tip Z.

Measurements of the secondary tip positions X_{tip} have been performed on the 2D reconstructions of the images obtained at different times for various supercoolings ($\Delta T = 0.287$, 0.370, 0.470, and 0.609 K). For a comparison of the data from different supercoolings, we use the tip radius R as a length scale to reduce the lengths X and Z. Figure 7 shows an example of such an envelope obtained according to the above-mentioned method at a supercooling of 0.370 K. It can be seen that the shape of the envelope does not change at different times and is very symmetrical relative to the primary stem axis. The envelopes for other supercoolings show the same behavior. Therefore, taking into account all data obtained at different times for both sides of a dendrite at all supercooling levels, the normalized envelope width X/R is plotted against the normalized distance away from the tip Z/R on a log-log scale in Fig. 8.

For $Z/R < 10$, the data points actually represent the contour of the tip region where no sidebranching occurs. It can be clearly seen from Fig. 8 that the shape of the tip region is closer to Brener's nonaxisymmetric needle crystal [21] than to a parabola and strongly differs from that measured far from the tip. Of course, an accurate measurement of the dendrite tip shape needs much higher resolution images and is beyond the scope of this paper. Here we restrict our attention to the sidebranching region.

For $Z/R > 10$, a least-squares fit of the data, indicated by the line drawn in Fig. 8, shows that from a distance Z/R

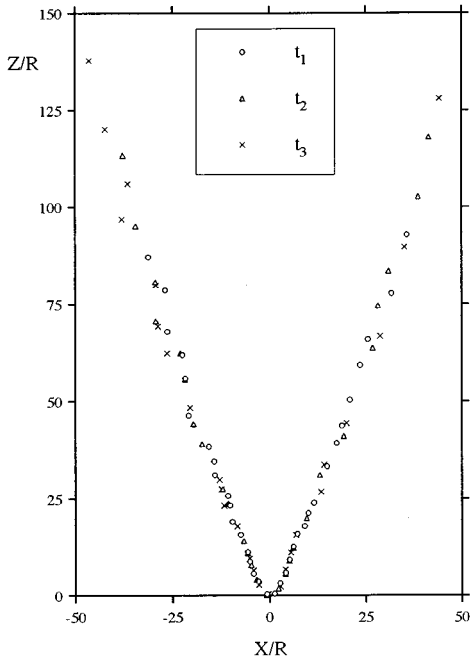

FIG. 7. Envelope delineated by active secondary arm tips ($\Delta T = 0.370$ K).

$=10$ to 250 (our maximum measurement range for the highest supercooling), the secondary tip positions for all dendrites can be correlated by

$$X_{\text{tip}}/R = 0.668(Z/R)^{0.859} \tag{4.1a}$$

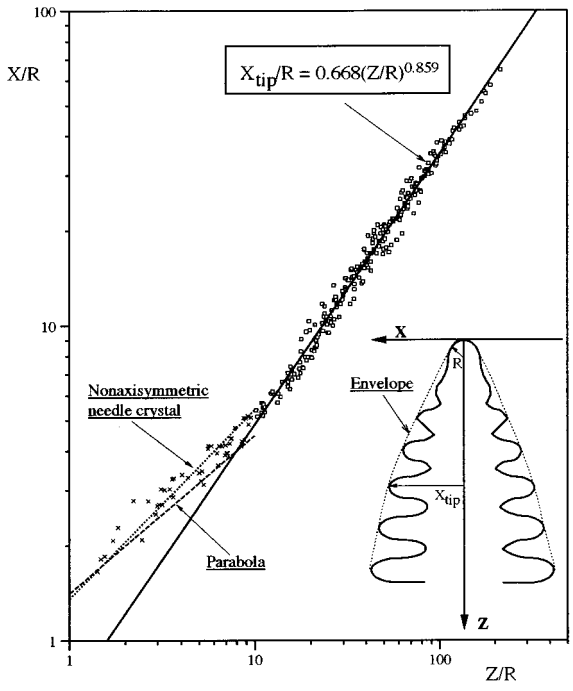

FIG. 8. Scaling relation between the normalized envelope width X/R and the normalized distance away from the tip Z/R. The symbols represent all data obtained at different times for both sides of a dendrite at four supercooling levels ($\Delta T = 0.287$, 0.370, 0.470, and 0.609 K). Only the squares were used for fitting the scaling relation.

or in terms of the secondary tip velocities v_2,

$$v_2 = 0.574 v_t (Z/R)^{-0.141}, \tag{4.1b}$$

where v_t is the speed of the primary tip. This result demonstrates that the dendrite envelope, like the tip region, behaves as a shape-preserving steady-state growth shape, at least on the sidebranch plane. This conclusion has an important implication for some models of equiaxed solidification such as Beckermann and Wang's multiphase model [33], because the envelope is no longer hypothetical but a meaningful interface that can be mathematically characterized by a growth law.

The maximum measurement range varies from about $Z/R = 80$ for $\Delta T = 0.287$ K to $Z/R = 250$ for $\Delta T = 0.609$ K. Using the tip radii and velocities in Table I and $\alpha = 1.128\ 10^5$ μm^2/sec [4], the corresponding inverse tip Péclet numbers 1/Pe vary from 450 (for $\Delta T = 0.287$ K) to 205 (for $\Delta T = 0.609$ K). Hence most of our experimental data are well within the range $1 \ll Z/R \ll 1/\text{Pe}$, for which self-similar sidebranching behavior was predicted by Brener and Temkin [25]. Interestingly, the data that are beyond this regime still follow the same scaling relation (see Fig. 8).

Comparing our experimental result $X_{\text{tip}}/R = 0.668(Z/R)^{0.859}$ with the theoretical prediction of the scaling exponent of unity predicted by Brener and Temkin [26] for the length of the survived (or active) sidebranches as a function of the distance from the tip [see Eq. (2.5)], it can be seen that the present sidebranches grow somewhat more slowly than predicted. This discrepancy probably comes from the fact that the Z component of the heat flux is neglected in the heat conservation equation leading to the scaling relation given by Eq. (2.5). In fact, the sidebranches do not grow normally to the primary dendrite stem (Z axis). Instead, they always follow the steepest thermal gradient normal to the ridges of the four fins of the needle crystal. We have estimated that for $20 < Z/R < 250$ the Z component of the heat flux varies from 24% to 9%. Therefore, the difference of 0.14 in the measured and predicted scaling exponents for the envelope shape is not surprising. Recently, we have numerically solved the three-dimensional heat equation in the liquid around the envelope of a sidebranching dendrite and found excellent agreement between the predicted envelope shape and the present scaling relation [33].

In order to compare with the experiments of Hurlimann *et al.* [20], where the amplitude of the sidebranches h_p (i.e., the normal distance between the secondary arm tips and a parabola fitted to the primary dendrite tip) was measured as a function of the parabola length l_p (see Fig. 6), we have transformed our experimental result $X_{\text{tip}}/R = 0.668(Z/R)^{0.859}$ into a relationship between h_p and l_p. This transformation does not have a closed-form analytical solution, but can be easily performed numerically. The result is shown as a series of dots in Fig. 9. For the range given by $15 < l_p/R < 300$ the measurements can be well fitted by a linear function

$$h_p/R = 0.222(l_p/R) - 2.32. \tag{4.2}$$

This result differs strongly from the one obtained by Hurlimann *et al.* for xenon dendrites: $h_p/R = 2.8 \times 10^{-3}(l_p/R)^{1.78}$. However, the linear relation between h_p and l_p agrees with the theoretical prediction of Brener and Temkin [25] that the scaling exponent is unity (see above).

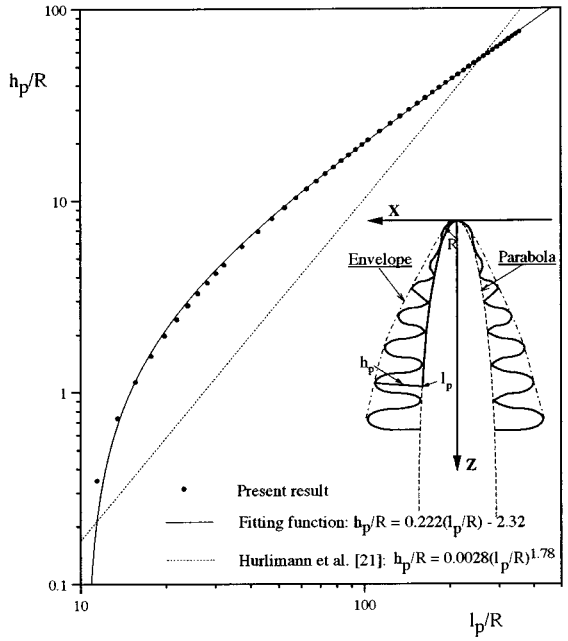

FIG. 9. Amplitude of sidebranches versus the length of the parabola normalized with the tip radius R (a comparison between the present result and that of Hurlimann *et al.*).

Since h_p and l_p in parabolic coordinates correspond to X and Z in Cartesian coordinates, respectively, the approximations that lead Brener and Temkin to obtain the scaling exponent of unity for the length of the survived sidebranches as a function of Z appear to be more suitable in the framework of parabolic coordinates. Note that the neglect of the Z component of the heat flux is less severe in parabolic coordinates.

B. Length of the contour and area of projection

Measurements of the contour length U and the projection area F have been performed at different times and different supercooling levels according to the method described in Sec. III. We focus on the scaling relationship between these two parameters and the distance away from the tip Z, which is equivalent to time $t=Z/v_t$. The length U is reduced by the tip radius R and the area F is normalized by R^2 in order to detect similarity for different supercoolings. Figures 10 and 11 give the results of the measurements at four different supercooling levels in a log-log plot.

It can be seen from Fig. 10 that all data for the normalized projection area F/R^2 coincide for different supercoolings and can be fitted by a power law

$$F/R^2 = 0.605(Z/R)^{1.70} \tag{4.3a}$$

or in terms of time

$$F/R^2 = 0.605(v_t t/R)^{1.70}. \tag{4.3b}$$

This result shows that the projection area F, if scaled by R^2, has a supercooling independent relation with the normalized distance Z/R (or time $v_t t/R$), which can be well represented from $Z/R=20$ to 250 by one power law. It implies that even such integral parameters as area can be scaled with R.

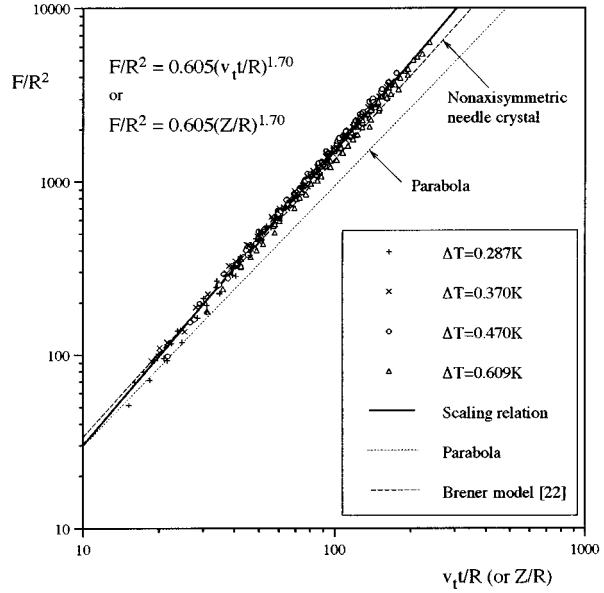

FIG. 10. Normalized projection area F/R^2 versus normalized time $v_t t/R$ (or Z/R).

For comparison, we include in Fig. 10 the behavior of $F(Z)$ for the nonaxisymmetric needle crystal of Brener [21], which can be written as

$$F/R^2 \approx 0.85(Z/R)^{1.6}. \tag{4.4}$$

It can be seen that the experimental scaling exponent of 1.70 is quite close to the theoretical scaling exponent of 1.6 for the nonaxisymmetric needle crystal of Brener [21]. This reflects the fact that conservation laws require the projection area of the needle crystal to be about the same as for a real dendrite with sidebranches. The difference of 0.1 between the experimental exponent and the theoretical prediction could be attributed to coarsening, which makes the primary

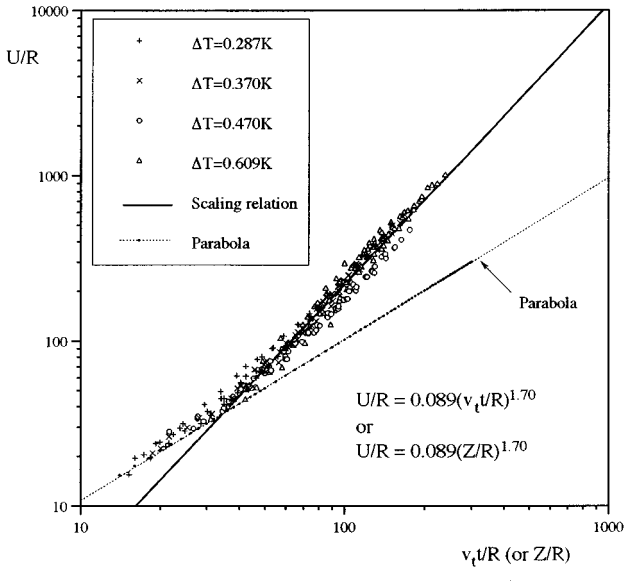

FIG. 11. Normalized contour length U/R versus normalized time $v_t t/R$ (or Z/R).

stem thicken in diameter by filling in the liquid ''troughs'' between the branches, as already observed by Huang and Glicksman [4].

The data for the contour length U, shown in Fig. 11, seem to also demonstrate a supercooling-independent behavior, although the data for $\Delta T=0.470$ K somewhat deviate from the others. Nevertheless, within the present measurement accuracy it is reasonable to consider the relationship between the normalized contour length U/R and the normalized time $v_t t/R$ (or Z/R) as supercooling independent.

Unlike F/R^2, the contour length U cannot be fitted by one power law over the entire measurement region ($10<Z/R<250$). Only for $Z/R>50$ can U/R be correlated to Z/R by

$$U/R=0.089(Z/R)^{1.70}. \tag{4.5}$$

The difference in the fitting range can be explained by comparing the behaviors of $F/R^2(Z/R)$ and $U/R(Z/R)$ for a parabolic dendrite, which are represented by dashed lines in Figs. 10 and 11, respectively. For a parabolic dendrite, the projection area F is given by

$$F/R^2=\frac{\sqrt{2}}{1.5}(Z/R)^{1.5}\approx 0.94(Z/R)^{1.5}. \tag{4.6}$$

It can be seen that there is no large difference between Eqs. (4.6) and (4.3a) in the tip region. This means that $F/R^2(Z/R)$ can easily change from the initial tip behavior, $F/R^2=0.94(Z/R)^{1.5}$, to the steady-state sidebranching behavior, $F/R^2=0.605(Z/R)^{1.70}$. On the other hand, the behavior of $U/R(Z/R)$ for a parabolic dendrite, which is given by

$$\frac{U}{R}=\frac{1}{2}\left[\sqrt{2\frac{Z}{R}\left(1+2\frac{Z}{R}\right)}+\ln\left(\sqrt{2\frac{Z}{R}}+\sqrt{1+2\frac{Z}{R}}\right)\right]\approx 1.14\left(\frac{Z}{R}\right)^{0.977}, \tag{4.7}$$

shows a large difference from that of a sidebranching dendrite in the region away from the tip [see Fig. 11 and Eq. (4.5)]. Therefore, $U/R(Z/R)$ changes later from the tip behavior to the sidebranching behavior.

A comparison between the exponents of the power laws (4.3a) and (4.5), shows that U/R and F/R^2 have the same time (or Z/R) dependence for $Z/R>50$. Dividing Eq. (4.5) by Eq. (4.3a) yields

$$\frac{U/R}{F/R^2}=0.147. \tag{4.8}$$

The above equation indicates that after an initial transient ($Z/R>50$), F increases linearly with increasing U. The slope m in the linear equation $F=mU$ can be scaled by the tip radius R, resulting in a normalized slope of $m/R=6.8$. This result is in fair agreement with the data of Hurlimann *et al.* for xenon dendrites [20], for which they found that $m/R=4$.

The linear dependence $F=mU$ can be illustrated by plotting the normalized ratio of RU/F versus the normalized time $v_t t/R$ (or Z/R) (Fig. 12) for all data obtained at the four

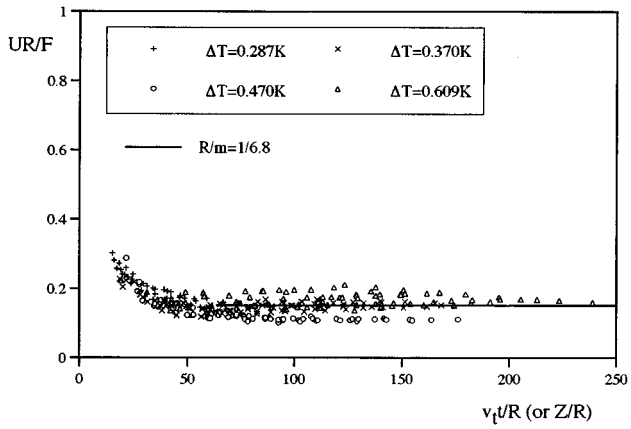

FIG. 12. Normalized ratio of contour length to projection area UR/F versus normalized time $v_t t/R$ (or Z/R).

supercoolings. Figure 12 confirms that after an initial transient stage ($Z/R>50$), UR/F becomes a time-independent constant.

Hurlimann *et al.* [20] have developed a simple model, called a rod model, to explain the linear behavior of $F(U)$. In this model, the primary stem and the sidebranches are approximated by cylindrical rods with the same diameter. Although this simple model successfully predicts a linear relationship between F and U, a more physical understanding of the observed behavior has yet to be obtained.

It should be noted that the ratio of U/F actually represents an interfacial length concentration. It has the same dimension (mm^{-1}) as the interfacial area concentration S and may qualitatively reflect the behavior of S. The experimental finding $U/F=0.147/R$ implies that the larger the supercooling ΔT, the higher the interfacial length or area concentration. This is compatible with the observation that a dendrite grown at a higher supercooling exhibits a finer structure.

C. Surface area and volume

In Sec. IV B we have confirmed that the projection area F and contour length U are well-reproducible quantities that describe the overall behavior of dendrites far from the tip. To obtain more information about dendrites it is necessary to study the volume and surface area in three dimensions. Since the direct measurement of the volume and surface area during growth is not possible, we can only estimate their values according to the method discussed in Sec. III.

The formulas for calculating the volume V and surface area A of a dendrite are provided in Sec. III. The sidebranch length L_i, tip radius R, and sidebranch spacing λ_i can be considered as experimental input in the estimate of the volume and surface area of the dendrites. This guarantees that the present calculations are principally based on experimental measurements.

Figures 13 and 14 give the results of the calculations by plotting the normalized volume V/R^3 and normalized surface area A/R^2 versus the normalized distance (or time) Z/R ($=v_t t/R$), respectively. Fitting the data for $Z/R>30$ by a power law, we found that the behavior of the volume can be described by

$$V/R^3=2.70(Z/R)^{2.10} \tag{4.9}$$

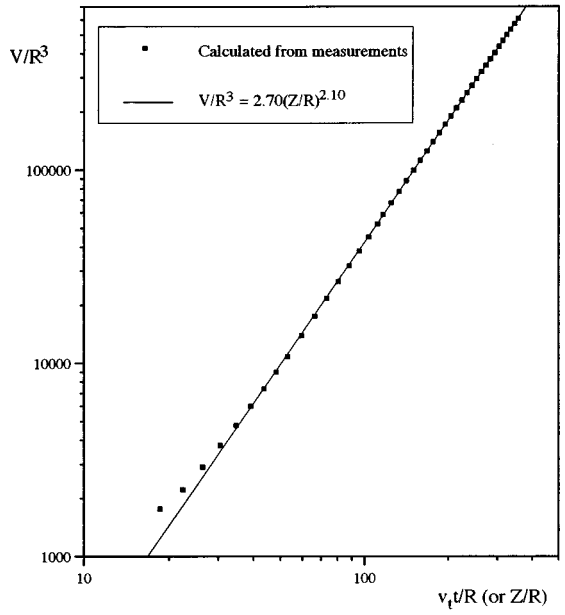

FIG. 13. Normalized dendrite volume V/R^3 versus normalized time $v_t t/R$ (or Z/R).

and that of the surface area A by

$$A/R^2 = 1.83(Z/R)^{1.92}. \tag{4.10}$$

Our measurements clearly indicate that the tip radius R is the only scaling parameter for the volume and surface area of dendrites far from the tip. By comparing Eq. (4.9) with the experimental finding $V \propto RL^3$ of Hurlimann *et al.* [20], we note that our estimate $V = 2.70R^{0.9}Z^{2.10}$ has a different distance dependence ($V \propto Z^{2.10}$) but has a similar, close to linear, relation to R. Note that our relation appears to be more plausible because $R^{0.9}Z^{2.1}$ has units of m^3. The discrepancy

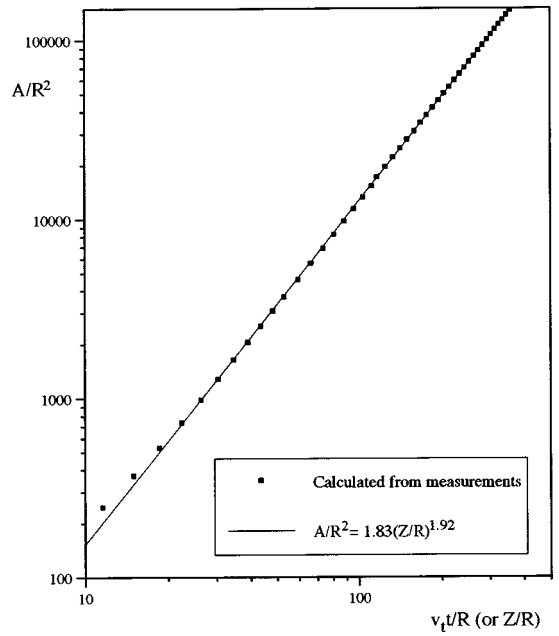

FIG. 14. Normalized dendrite surface area A/R^2 versus normalized time $v_t t/R$ (or Z/R).

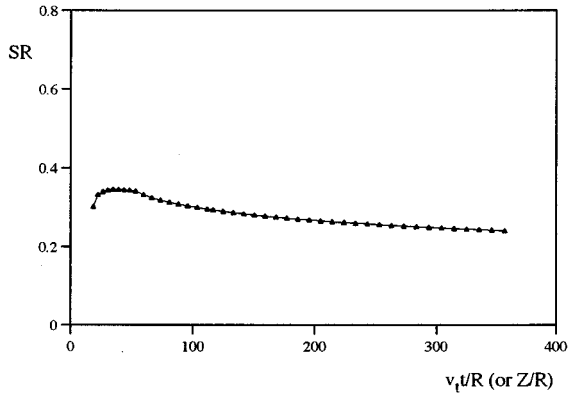

FIG. 15. Normalized interfacial area concentration SR versus normalized time $v_t t/R$ (or Z/R).

with the Hurlimann *et al.* relation probably arises from the fact that the length L was taken as the distance between the primary tip and the end of the stinger, which includes a strong thermal interaction region at the root of dendrite. In our case, the length Z is defined as the distance away from the tip and is within the range of no thermal interactions with another primary stem.

The scaling exponent of 2.10 for the volume (4.9) is close to the fractal dimension of a three-dimensional dendrite, which is simply equal to 2. It is possible that the difference is due to the approximations made in estimating the volume from the measurements (see Sec. III). However, it is shown below in Sec. IV D that within the range of the present measurements a scaling exponent of 2.10 results in better agreement with a heat transfer model than an exponent of 2 would.

From Eqs. (4.9) and (4.10) we can deduce the behavior of the interfacial area concentration S as

$$S = \frac{A}{V} = 0.68\,\frac{1}{R}\,(Z/R)^{-0.18}. \tag{4.11}$$

The above result shows that the interfacial area concentration S is inversely proportional to the tip radius R and slowly decreases with increasing Z/R. This behavior can be more directly illustrated by plotting the normalized interfacial area concentration SR versus Z/R, as shown in Fig. 15. The exponent -0.180 is close to the value of -0.25 predicted by Langer [19] for the distance dependence of the wavelength of the sidebranch instability [see Eqs. (2.1) and (3.3)] that we used in the present estimates of the surface area and volume. Substituting Eq. (3.4) into Eq. (4.11) yields

$$S = 1.15\,\frac{1}{\lambda}\,(Z/R)^{0.07}. \tag{4.12}$$

The exponent on Z/R is so small (0.07) that the distance dependence in Eq. (4.12) may be neglected. Then Eq. (4.12) implies that the interfacial area concentration is inversely proportional to the secondary arm spacing and may be approximated for $50 < Z/R < 300$ by

$$S \approx \frac{1.6}{\lambda}. \tag{4.13}$$

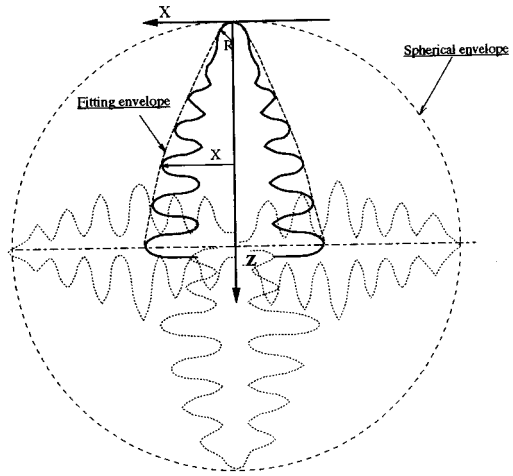

FIG. 16. Schematic illustration of different envelopes of a dendrite (2D cross section).

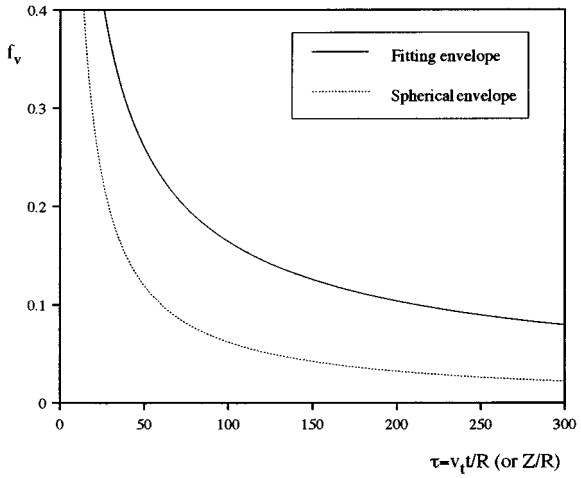

FIG. 17. Volume fraction versus normalized growth distance for different envelopes.

This result is consistent with the commonly employed simple one-dimensional plate model of secondary dendrite arms [34], although the constant of proportionality is somewhat different from 2.

A comparison between the interfacial area concentration S and the interfacial length concentration (U/F) shows that both of them behave similarly. In fact, the relatively weak dependence of S on Z/R in Eq. (4.11) suggests that the interfacial area concentration S, like the interfacial length concentration, can be approximated as a constant with respect to the distance Z/R. In the range $100 \leqslant Z/R \leqslant 300$, Eq. (4.11) gives $S = 0.3/R \sim 0.25/R$, which is consistent with the interfacial length concentration relation $U/F = 0.15/R$ and closer to the result of Hurlimann *et al.*, $U/F = 0.25/R$. This comparison suggests that the interfacial area concentration S and the interfacial length concentration are two equivalent parameters.

D. Volume fraction

In modeling solidification systems involving multiple equiaxed crystals, the fraction solid inside certain crystal envelopes is a more useful parameter than the volume of a single sidebranching dendrite arm, as given by Eq. (4.9) [34]. Therefore, we have calculated the solid volume fraction for two different envelopes: a fitting envelope and a spherical envelope. The fitting envelope is defined as a revolution of the secondary tip envelope on the sidebranch plane around the Z axis, as shown in Fig. 16. Its volume can be determined from Eq. (4.1a) through an integration

$$\frac{V_{\text{fit}}}{R^3} = \int_0^{Z/R} \pi \left(\frac{X}{R}\right)^2 dZ \approx 0.964 \left(\frac{Z}{R}\right)^{2.72}. \tag{4.14a}$$

The spherical envelope is chosen to correspond to an entire equiaxed crystal consisting of six orthogonal primary arms (see Fig. 16). Since Eq. (4.9) gives the dendrite volume for one primary arm only, it is multiplied by 6 to approximate the volume of a whole crystal. The radius of the spherical envelope is taken to be the length of a primary arm; hence

$$\frac{V_{\text{sph}}}{R^3} = \frac{4}{3}\,\pi \left(\frac{Z}{R}\right)^3 = \frac{4}{3}\,\pi \left(\frac{v_t t}{R}\right)^3. \tag{4.14b}$$

Introducing the formula for the dendrite volume [Eq. (4.9)], the volume fractions for the two envelopes are given by

$$f_{v\ \text{fit}} = \frac{V}{V_{\text{fit}}} = 2.80(Z/R)^{-0.62}, \tag{4.15a}$$

$$f_{v\ \text{sph}} = \frac{V}{V_{\text{sph}}} = 3.86(Z/R)^{-0.90}. \tag{4.15b}$$

The variation of the two volume fractions are plotted in Fig. 17 as a function of the normalized distance away from the tip Z/R for both the fitting envelope and the spherical envelope. It can be seen that the volume fraction decreases with the growth distance Z (or the growth time t). Obviously, the fitting envelope generally results in higher volume fractions than the spherical envelope. While Eqs. (4.15) are scaling relations valid for any supercooling, the actual distance (or time) dependence changes with the tip radius and hence supercooling.

The variation of the volume fraction for an equiaxed crystal inside a spherical envelope can be easily explained by adapting a previously developed model of equiaxed solidification [34]. In this model, the liquid and solid inside the spherical envelope are assumed to be uniformly at the melting temperature and any growth occurs by heat conduction at the envelope into the surrounding supercooled liquid. Hence an energy balance at the envelope surface can be written as

$$A_{\text{sph}} k \frac{\Delta T}{\delta} = L\rho \left(V_{\text{sph}} \frac{df_v}{dt} + f_v \frac{dV_{\text{sph}}}{dt} \right), \tag{4.16}$$

where A_{sph} is the surface area of the spherical envelope, k is the thermal conductivity, L is the latent heat, ρ is the density, ΔT is the supercooling, and δ is a heat diffusion length. Assuming quasisteady conditions and solving the differential equation governing heat diffusion around a growing sphere, it can be shown that the temperature profile in the liquid

outside the envelope is of an exponential nature and the heat diffusion length is given by [35]

$$\delta=\left[1-\exp\left(-\frac{v_t^2}{\alpha}t\right)\right]\frac{\alpha}{v_t}=[1-\exp(-2\,\mathrm{Pe}\tau)]\,\frac{\alpha}{v_t}, \tag{4.17}$$

where Pe is the tip Péclet number and τ is the dimensionless time $\tau=v_t t/R=Z/R$. Substituting Eq. (4.17) into Eq. (4.16) and making some rearrangements, we obtain

$$\frac{\tau}{3}\frac{df_v}{d\tau}+f_v=\Omega[1-\exp(-2\,\mathrm{Pe}\tau)]^{-1}, \tag{4.18}$$

where $\Omega=\Delta T/(L/c)$ is the dimensionless supercooling and c is the specific heat. For SCN, $L/c=23.8$ K [4]. An initial condition for Eq. (4.18) can be obtained by setting the volume of six paraboloidal dendrite tips of length $Z=v_t t$ equal to the volume of a spherical envelope of radius $v_t t$, which yields that $f_v=1$ at $\tau=4.5$. However, we found that the solution is insensitive to the initial condition for $\tau\geqslant 10$. For $\tau\ll 1/\mathrm{Pe}$, an approximate solution of Eq. (4.18) can be obtained by setting $\exp(-2\,\mathrm{Pe}\tau)\approx 1-2\,\mathrm{Pe}\tau$ and is given by

$$f_v=\frac{3}{4}\frac{\Omega}{\mathrm{Pe}}\tau^{-1}+91.125\left(1-\frac{\Omega}{6\,\mathrm{Pe}}\right)\tau^{-3}. \tag{4.19}$$

For $\tau>20$, the last term in Eq. (4.19) can be neglected, indicating that the volume fraction varies with τ^{-1}. Within the present supercooling range (see Table I), the prefactor $(3\Omega/4\,\mathrm{Pe})$ ranges from 4.1 to 3.9, showing that the supercooling dependence is weak. In fact, for $\mathrm{Pe}\ll 1$ the Ivantsov solution [23] behaves as $\Omega\sim\mathrm{Pe}$. Hence, within the self-similar regime $1\ll\tau\ll 1/\mathrm{Pe}$, the approximate solution (4.19) is indeed supercooling independent. Furthermore, the scaling exponent of -1 from the approximate solution of the heat transfer model is reasonably close to the experimental value (i.e., -0.9).

In order to verify the above approximate solution and to illustrate the long-time behavior of the heat transfer model, we also solved Eq. (4.18) numerically. Figure 18 shows the model predictions computed for the four supercoolings used in the present analysis (Table I) and compares them to the experimental correlation (4.15b) as well as to the approximate solution $f_v\approx 4\tau^{-1}$. Although we plot the experimental correlation up to $\tau=300$, it should be kept in mind that it is only valid up to $\tau\ll 1/\mathrm{Pe}$ and that 1/Pe is smaller than 300 for the higher supercoolings (e.g., $1/\mathrm{Pe}=205$ for $\Delta T=0.609$ K; see Sec. IV A). It can be seen that for $\tau\ll 1/\mathrm{Pe}$, the numerically predicted variation of the volume fraction f_v with τ is virtually supercooling independent. The agreement between the numerical solution of the heat transfer model and the experimental correlation is good. For $30<\tau\ll 1/\mathrm{Pe}$, the fitting range of the present volume measurements, the scaling exponent that can be surmised from the plot of the numerical solution in Fig. 18 is closer to the experimental value of -0.9 than to the value of -1 from the approximate solution given by the first term of Eq. (4.19). Hence the heat transfer model provides a reasonable explanation why the scaling exponent for the volume measurements (i.e., 2.1) [Eq. (4.9)] is somewhat larger than the theoretical value of 2 (see Sec. IV C). At larger times, corresponding to $\tau\geqslant 1/\mathrm{Pe}$ the numerically predicted volume fraction variation becomes supercooling dependent and approaches a constant value that is given by

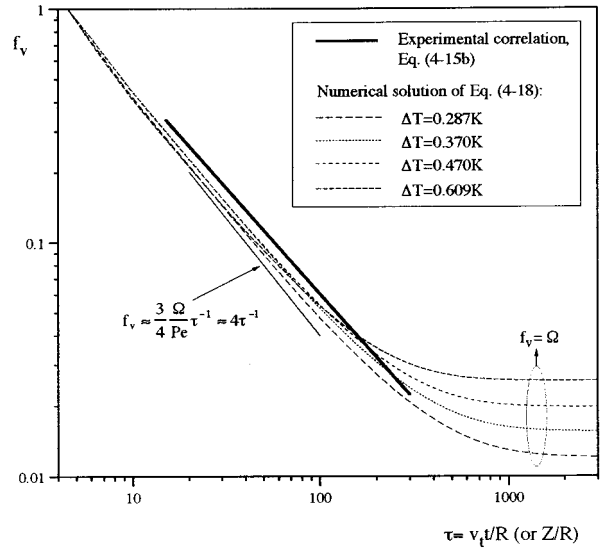

FIG. 18. Measured volume fractions for a spherical envelope (a comparison between theoretical prediction and measurement results).

$$f_v=\Omega. \tag{4.20}$$

This result simply states that in steady growth of an equiaxed crystal, the sensible heat available in the supercooled melt is converted into latent heat to produce a dendritic crystal of a certain internal solid volume fraction. Although the SCN dendrites in the IDGE were generally grown for several millimeters in length, no experimental data are available to verify the predicted long-time behavior. Nonetheless, the good agreement at earlier times establishes considerable confidence in both the present measurements and the model. It should be noted that variations of the above model are quite popular in the simulation of microstructures in equiaxed alloy castings [34], but they have never been validated by experimental measurements, as is done here.

V. CONCLUSIONS

A detailed measurement of the morphology of pure succinonitrile dendrites is performed using images from the first microgravity flight of the IDGE to investigate the scaling behavior of geometry parameters in three-dimensional dendritic growth. The results presented in this paper show that unique scaling relations exist between the geometry parameters and the primary tip radius in steady growth. The scaling relations are valid in the nonlinear, self-similar sidebranching region far from the primary tip $1\ll Z/R\ll 1/\mathrm{Pe}$.

For the secondary arm envelope on the sidebranch plane, the envelope width (or the secondary dendrite tip position) X_{tip} can be correlated to the distance away from the primary tip Z according to $X_{\mathrm{tip}}/R=0.668(Z/R)^{0.859}$. This indicates that the dendrite envelope growth is a shape-preserving steady-state process. If the above relation is converted to

parabolic tip coordinates, the length of the surviving secondary dendrite arms is found to vary linearly with distance from the tip, which is in agreement with the analysis of Brener and Temkin [25].

The projection area F and the contour length U of a dendrite on the sidebranch plane, after scaling by R^2 and R, respectively, have their own supercooling-independent relation with Z/R. After a transient stage, both of them can be described by a power law with the same exponent of 1.70, demonstrating the same time dependence. This result implies that the interfacial length concentration U/F is time independent, after some initial transient, and inversely proportional to the tip radius R. The exponent 1.7 is in reasonable agreement with the theoretical value of 1.6 derived by Brener and Temkin [25].

Calculations of the volume V and the surface area A of a dendrite, based on the experimental measurements and some approximations, show that these parameters can also be scaled to the tip radius R. The scaling exponent for the volume is close to the theoretical value of 2. The interfacial area concentration A/V, deduced from the above calculations, demonstrates a relatively weak time dependence. Averaged over time, A/V shows a similar behavior and the same order value as the interfacial length concentration U/F.

Solid volume fractions for two different envelopes (a fitting envelope and a spherical envelope) have also been estimated. In our measurement range, the volume fractions for these two envelopes decrease with the normalized growth time $v_t t/R$ in a supercooling-independent manner. For the spherical envelope, the volume fraction variation based on the measurements is in good agreement with predictions from a simple heat transfer model.

ACKNOWLEDGMENTS

This work was supported by NASA under Contract No. NCC8-94. The authors are indebted to Professor Glicksman of RPI and NASA for making the IDGE images available to us. We also thank Kai Liu for his help with numerical calculations.

[1] J. S. Langer, Rev. Mod. Phys. **52**, 1 (1980).
[2] J. S. Langer, Science **243**, 1150 (1989).
[3] M. Ben Amar and Y. Pomeau, Europhys. Lett. **2**, 307 (1986).
[4] S. C. Huang and M. E. Glicksman, Acta Metall. **29**, 701 (1981); **29**, 717 (1981).
[5] A. Dougherty and J. P. Gollub, Phys. Rev. A **38**, 3043 (1988).
[6] X. W. Qian and H. Z. Cummins, Phys. Rev. Lett. **64**, 3038 (1990).
[7] J. S. Langer, in *Chance and Matter*, Proceedings of the Les Houches Summer School of Theoretical Physics, Session XLVI, edited by J. Souletie, J. Vannimenus, and R. Stora (North-Holland, Amsterdam, 1987), p. 629.
[8] D. Kessler, J. Koplik, and H. Levine, Adv. Phys. **37**, 255 (1988).
[9] Y. Pomeau and M. Ben Amar, in *Solids Far From Equilibrium*, edited by C. Godreche (Cambridge University Press, Cambridge, 1992).
[10] M. E. Glicksman, M. B. Koss, and E. A. Winsa, Phys. Rev. Lett. **73**, 573 (1993).
[11] G. R. Kotler and W. A. Tiller, J. Cryst. Growth **2**, 287 (1968).
[12] J. S. Langer and H. Müller-Krumbhaar, Acta Metall. **26**, 1681 (1978).
[13] J. S. Langer and H. Müller-Krumbhaar, Acta Metall. **26**, 1689 (1978).
[14] H. Müller-Krumbhaar and J. S. Langer, Acta Metall. **26**, 1697 (1978).
[15] A. Dougherty, P. D. Kaplan, and J. P. Gollub, Phys. Rev. Lett. **58**, 1652 (1987).
[16] Ph. Bouissou, A. Chiffaudel, B. Perrin, and P. Tabeling, Europhys. Lett. **13**, 89 (1990).
[17] A. Barbieri, D. Hong, and J. S. Langer, Phys. Rev. A **35**, 1802 (1987).
[18] M. N. Barber, A. Barbieri, and J. S. Langer, Phys. Rev. A **36**, 3340 (1987).
[19] J. S. Langer, Phys. Rev. A **36**, 3350 (1987).
[20] E. Hurlimann, R. Trittibach, U. Bisang, and J. H. Bilgram, Phys. Rev. A **46**, 6579 (1992).
[21] Efim Brener, Phys. Rev. Lett. **71**, 3653 (1993).
[22] M. Ben Amar and Efim Brener, Phys. Rev. Lett. **71**, 589 (1993).
[23] G. P. Ivantsov, Dokl. Akad. Nauk SSSR **58**, 567 (1947).
[24] R. Almgren, W. S. Dai, and V. Hakim, Phys. Rev. Lett. **71**, 3461 (1993).
[25] E. Brener and D. Temkin, Phys. Rev. E **51**, 351 (1995).
[26] U. Bisang and J. H. Bilgram, Phys. Rev. Lett. **75**, 3898 (1995).
[27] U. Bisang and J. H. Bilgram, Phys. Rev. E **54**, 5309 (1996).
[28] M. E. Glicksman, M. B. Koss, L. T. Bushnell, J. C. LaCombe, R. N. Smith, and E. A. Winsa, in *Heat Transfer in Microgravity Systems*, edited by S. S. Sadhal and A. Gopinath (ASME, New York, 1994), Vol. 290, pp. 1–8.
[29] M. E. Glicksman, M. B. Koss, L. T. Bushnell, J. C. LaCombe, and E. A. Winsa, ISIJ Int. **35**, 1216 (1995).
[30] M. E. Glicksman, M. B. Koss, L. T. Bushnell, J. C. LaCombe, and E. A. Winsa, AIAA Report No. 96-0251, 1996 (unpublished).
[31] J. C. LaCombe, M. B. Koss, V. E. Fradkov, and M. E. Glicksman, Phys. Rev. E **52**, 2778 (1995).
[32] Q. Li and C. Beckermann (unpublished).
[33] I. Steinbach, B. Kauerauf, C. Beckermann, and J. Guo, in *Solidification 97*, edited by J. A. Dantzig and S. P. Marsh (TMS, Warrendale, PA, in press).
[34] C. Beckermann and C. Y. Wang, in *Annual Review of Heat Transfer*, edited by C. L. Tien (Begell House, New York, 1995), Vol. 6, pp. 115–198.
[35] C. Y. Wang and C. Beckermann, Metall. Trans. A **24**, 2787 (1993).